Results in Physics 15 (2019) 102653

Contents lists available at ScienceDirect

Results in Physics

journal homepage: www.elsevier.com/locate/rinp

Uniaxial magnetization reversal process in electrodeposited high-density iron nanowire arrays with ultra-large aspect ratio

Cornelia Neetzel[a,1], Himeyo Kamimura[a], Masamitsu Hayashida[a], Takeshi Ohgai[a,*]

[a] Graduate School of Engineering, Nagasaki University, Bunkyo-machi 1-14, Nagasaki 852-8521, Japan

ARTICLE INFO

Keywords:
Anodization
Aluminum oxide
Nanochannel
Electrodeposition
Iron
Nanowires
Magnetization
Reversal
Curling
Coercivity
Squareness

ABSTRACT

In this study, magnetization reversal modes of iron nanowire arrays with large aspect ratios were investigated by Shtrikman's micromagnetic theory. The iron nanowire arrays were potentiostatically electrodeposited into anodized aluminum oxide nanochannels with average diameters, D_p, of ca. 33 nm, 52 nm, 67 nm, and 85 nm. The growth rate of the iron nanowires was ca. 105 nm s^{-1} at the cathode potential of −1.2 V (vs. an Ag/AgCl reference), and the axial length, L_w, reached up to ca. 60 μm. Maximum aspect ratio, L_w/D_w of the iron nanowires was found to be ca. 1800, and the axial direction coincided with ⟨1 1 0⟩ direction of the bcc-Fe crystal structure. The effect of the average diameter size on the coercivity of iron nanowire arrays corresponded well to the theoretical estimate, which was calculated by the magnetization curling mode in Shtrikman's micromagnetic theory. As the average diameter of the iron nanowires was decreased, coercivity and squareness of the nanowire arrays increased up to 1.63 kOe and 0.87, respectively.

Introduction

Ferromagnetic iron nanostructures have been making important contributions to advanced materials research in recent years, particularly in fields such as biomedical science [1], electronic device manufacturing [2], sensor systems [3], and water treatment techniques [4]. It is well known that some iron-containing natural products, such as iron ores, can be found in a variety of combinations with other elements. In particular, iron can form ca. sixteen thermodynamically stable compounds with oxygen [5]. Scientists and engineers therefore often meet with many difficulties in the preparation of iron-based nanostructures with high purities, as iron is highly sensitive to oxidation and agglomeration, especially in oxidizing environments. In the production of one-dimensional nanostructures of only several tens of nanometers in length, several specialized advanced techniques are required in order to obtain nanostructures of precisely controlled geometries. To synthesize some nanostructured materials, several fabrication processes, including electrospinning [6], sol–gel [7], solvothermal synthesis [8], and template-based techniques [9,10] have been routinely used. Among them, template-based methods using films with numerous nanochannels, such as ion track etched polymer films [11] or anodized aluminum oxide (AAO) films [12,13], exhibit many advantages due to their excellent functionalities and ease of manufacture. In particular, AAO nanochannel films enable us to make nanowire arrays with high aspect ratios and high densities, which are derived from ultra-high porous structures in an AAO film. By controlling certain anodizing conditions, the porosity of an AAO film has been augmented to over 30% [14]. Usually, a template-based technique includes a two-step process, in which nanochannel films are synthesized first, and nanowire arrays are then electrochemically grown inside the nanochannels by electrodeposition [15,16] or electroless-deposition [17] techniques.

One of the crucial factors determining the physical properties of one-dimensional iron nanostructures is the average cross-sectional diameter, D_w, of the nanowires. Jia et al. [18] reported the effects of D_w on the coercivity, H_c and the squareness, and M_r/M_s of iron alloy nanowire arrays of ca. 18 μm in length (L_w). They found that H_c and M_r/M_s increased up to ca. 1.2 kOe and ca. 0.4, respectively, as D_w decreased down to ca. 30 nm (aspect ratio, L_w/D_w = ca. 600). Liu et al. [19] also investigated the effects of D_w on H_c and M_r/M_s of iron alloy nanowire arrays of ca. 4 μm in length. In their report, H_c and M_r/M_s increased up to ca. 2.0 kOe and ca. 0.9, respectively, as D_w decreased down to ca. 16 nm (L_w/D_w = ca. 250). Zeng et al. [20] also reported that the H_c of iron nanowires of ca. 5 μm in length strongly depended on D_w. They found that M_r/M_s reached ca. 0.9 and that H_c increased up to ca. 2.6 kOe as D_w decreased down to ca. 14 nm (L_w/D_w = ca. 360).

It is well known that the surface magnetic flux density, B, of a

* Corresponding author.
E-mail address: ohgai@nagasaki-u.ac.jp (T. Ohgai).
[1] (Presently) Freelancer: Patent Agent and Translator, Friedrich-Fendt-Straße 13, 63654 Büdingen, Germany.

https://doi.org/10.1016/j.rinp.2019.102653
Received 24 July 2019; Received in revised form 7 September 2019; Accepted 9 September 2019
Available online 11 September 2019

cylindrical magnet can be expressed by the following equation:

$$B = \frac{B_r}{2}\left\{\frac{L+z}{\sqrt{R^2+(L+z)^2}} - \frac{z}{\sqrt{R^2+z^2}}\right\} \quad (1)$$

if the B field is on the symmetrical axis of an axially magnetized cylindrical magnet.

Here, B_r is the remanence field, which is independent of the magnet's geometry. L is the axial length of the cylindrical magnet, and z is the distance from either pole face on the symmetrical axis. R is the cross-sectional radius of the cylindrical magnet.

Shtrikman et al. [21] theoretically investigated the effect of cross-sectional radius, R, on the H_c of an infinite ferromagnetic cylinder. In this model, the axial length of the cylinder is defined as infinity. Hence, the aspect ratio is also defined as infinity. They found that if R is larger than the critical radius size, R_c, for single-domain behavior, they estimated that H_c (in Oe) decreases with an increase in R (in cm) according to the following equation:

$$H_c = \frac{6.78A}{M_s R^2} \quad (2)$$

here, A (in erg/cm) is the exchange constant and M_s (in G) is the saturation magnetization.

As shown in Eqs. (1) and (2), B increases with an increase in L and H_c increases with a decrease in R. Thus, if magnetic nanowire arrays are applied for permanent magnetic materials with an anisotropic magnetization performance, an industrial production line will require magnetic nanowires of a higher density and aspect ratio. However, so far, the aspect ratios of iron nanowire arrays that have been reported by other researchers have not yet reached 1000.

Recently, our research group has reported that iron nanowires of ca. 60 μm in length and ca. 30 nm in diameter (aspect ratio L_w/D_w = ca. 2000) can be electrochemically grown from a bath containing 0.05 M $FeSO_4$ by using a pulsed-potential deposition technique [22]. We found that H_c and M_r/M_s reached up to ca. 1.4 kOe and ca. 0.95 when we controlled the crystal texture coefficients of iron nanowire arrays. In the present study, to determine the magnetization reversal mechanism of iron nanowire arrays with aspect ratios of over 1000, we investigated the effect of D_w on H_c based on a theoretical estimation, which was previously reported by Shtrikman et al. [21].

Experimental

AAO membrane preparation

AAO membranes were fabricated as previously described in the literature [22]. First, the rounded upper surface of an aluminum rod with a diameter of 1 cm was mechanically and electrochemically polished. The side surface of the rod was then covered with a polyimide tape. The anodization process was conducted in a 0.3 M oxalic acid solution at a constant temperature of 12 °C. Following anodization, porous foil was obtained by immersing the aluminum rod into a solution containing a mixture of ethanol and perchloric acid and applying an anodic potential 10 V higher than that used during the anodization process, for 3 s [23]. In order to obtain membranes with different pore sizes, anodization was carried out at 90, 70, 50, and 30 V. Because of the increased growth rate of the aluminum oxide layer at higher anodization voltages [24], anodization times were varied at 4.0, 5.5, 8.0, and 22 h, respectively, for the increasing voltage values. Using these variable durations, the membrane thicknesses were fixed to 60 μm each.

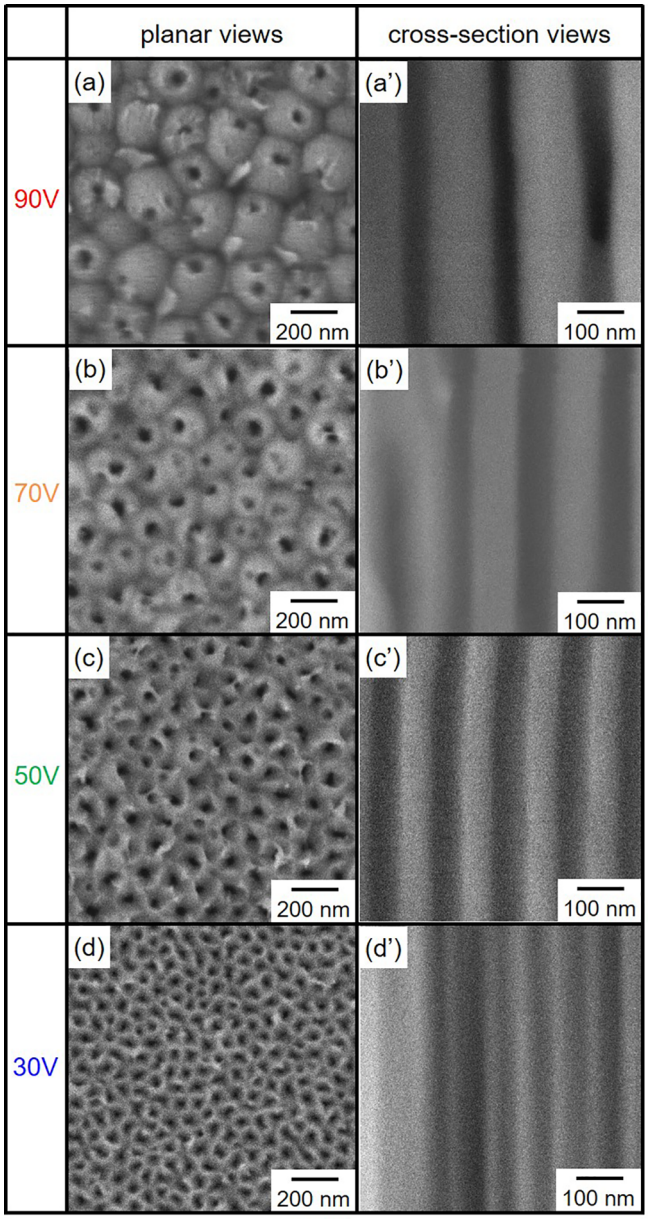

Fig. 1. SEM images of planar views and cross-section views of AAO nanochannel templates that were anodized at 90 V (a, a'), 70 V (b, b'), 50 V (c, c') and 30 V (d, d').

Electrodeposition of iron nanowires

To obtain a cathode starting layer, a thin gold film was sputter-deposited at 10 V for 900 s on one side of the membrane using a JEOL JFC-1600 ion sputtering device. Afterward, the conductive side was attached to a copper plate using silver paste and mechanically stabilized with polyimide tape. The electrodeposition of pure iron nanowire arrays was carried out in a 0.5 M iron sulfate heptahydrate electrolyte at a pH value of 2.0 and a constant temperature of 30 °C. The electrodeposition was carried out in a three-electrode assembly with Ag/AgCl as a reference and a thin gold wire serving as a counter electrode. A constant deposition potential of −1.2 V vs. Ag/AgCl was chosen.

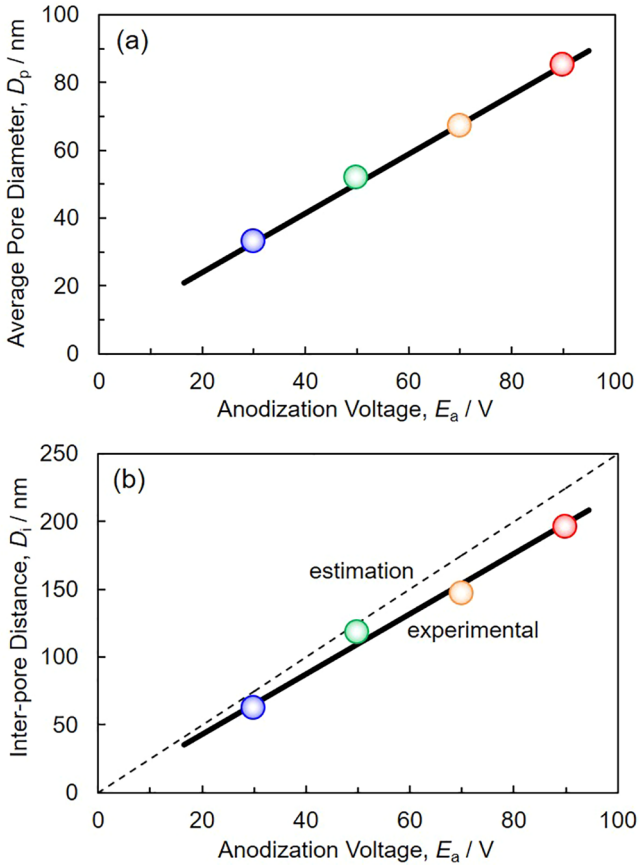

Fig. 2. Effect of anodization voltage on average pore diameter (a) and inter-pore distance (b) of AAO nanochannel templates.

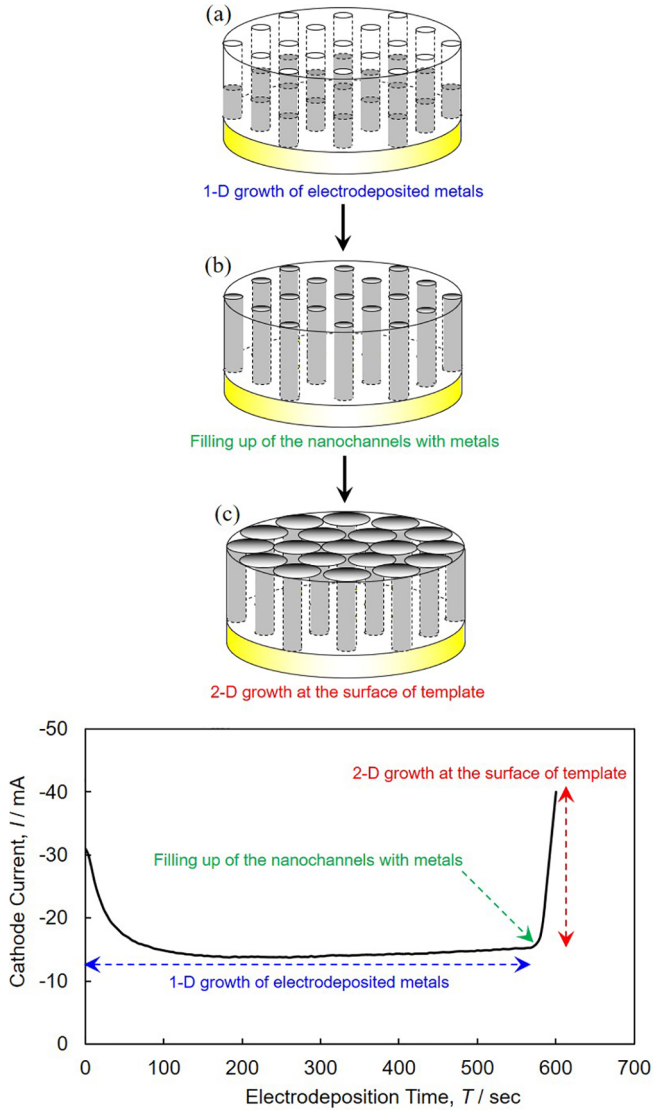

Fig. 3. Time-dependence of cathode current during the electrodeposition of iron nanowires in the nanochannels of an AAO template with the pore diameter of 33 nm.

Structure and magnetic properties of iron nanowires

After growing the iron nanowire arrays, the templates were dissolved in an aqueous solution containing 5 mol l^{-1} sodium hydroxide to separate the nanowires from the AAO membranes. Microstructures of the separated iron nanowire arrays were investigated by Scanning Electron Microscopy (SEM) and Transmission Electron Microscopy. The crystal orientation was also characterized using an X-ray Diffractometer. Magnetization curves of the arrays were obtained at room temperature using a vibrating sampling magnetometer with an external magnetic field of up to 10 kOe applied to the radial and axial directions of the nanowires. Here the radial direction is orthogonal to the long axis of the nanowires, while the axial direction is parallel to the long axis.

Results and discussion

Nanochannel structure of AAO films

Fig. 1 shows SEM images in planar views ((a), (b), (c), and (d)) and cross-sectional views ((a'), (b'), (c'), and (d')) of AAO membranes anodized at 30, 50, 70, and 90 V. According to the SEM images, it can be seen that the membranes have a through-hole architecture with holes oriented in parallel and no interconnections. It is well known that the AAO membrane structural parameters, such as interpore distance, pore diameter, and membrane thickness, depend on experimental conditions such as anodization voltage and solution temperature. According to one report [25], low temperature conditions produce smaller pore diameters, D_p, but do not show significant effects on interpore distances, D_i. By contrast, anodization voltage exerts strong effects on both the pore diameters, D_p, and the interpore distances, D_i. Several research groups have described that the interpore distance, D_i (in nm), is linearly proportional to the anodization voltage, E_a (in V), as shown in the following Eq. (3):

$$D_i = fE_a \tag{3}$$

where the factor of proportionality $f = 2.5$ (nm/V) [24,26,27]. This equation gives estimated interpore distances of 75, 125, 175, and 225 nm for anodization voltages of 30, 50, 70, and 90 V, respectively. These expected values were compared to the D_p and D_i values found by

Fig. 4. SEM image of electrodeposited iron nanowires, which were separated from an AAO nanochannel template with the pore diameter of 33 nm.

analyzing the SEM images in Fig. 1. The average pore diameters, D_p, from SEM analysis were $D_p^{30V} = 33$ nm, $D_p^{50V} = 52$ nm, $D_p^{70V} = 67$ nm, and $D_p^{90V} = 85$ nm, while the average interpore distances, D_i, were $D_i^{30V} = 62$ nm, $D_i^{50V} = 118$ nm, $D_i^{70V} = 147$ nm, and $D_i^{90V} = 196$ nm.

Fig. 2 shows the effects of anodization voltage on average pore diameter, D_p (a), and interpore distance, D_i (b), of AAO nanochannel templates. As shown in Fig. 2, pore diameters D_p and interpore distances D_i increase with increases in anodization voltage. In our experimental conditions, the factor of proportionality in Eq. (3), f, was determined to have been ca. 2.2 (nm/V) which is slightly lower than the estimated value.

Electrodeposition process and crystal structure of iron nanowires

Fig. 3 shows the time-dependence of cathodic current during the electrodeposition of iron nanowires in the nanochannels of an AAO template with a pore diameter of 33 nm. At the beginning of the electrodeposition (until ca. 50 s), the gradual decrease in cathodic current was observed because of a decreasing concentration of cations (Fe^{2+} and H^+) in the pores. In the following phase (ca. 50–550 s), a constant cathodic current (ca. 15 mA) was observed due to the stable diffusion and migration of cations from the bulk solution to the insides of the pores. It is well known that the termination of nanowire growth in the pores can be detected by a drastic increase in the cathodic current due to hemispheric cap formation on the surface of the membrane. This cap formation results in a rapid increase in the cathode's surface area. In the present work, a membrane with a thickness of ca. 60 μm was used as a template. Hence, the maximum length of iron nanowires reached ca. 60 μm. As shown in Fig. 3, the filling-up time was ca. 570 s. Therefore, the growth rate can be estimated to be ca. 105 nm s^{-1}.

Fig. 4 shows an SEM image of electrodeposited iron nanowires, which were separated from an AAO nanochannel template with a pore diameter of 33 nm. The one-dimensional structures with extremely large aspect ratios were densely packed, and each iron nanowire lay in a parallel direction. Fig. 5 shows TEM bright-field images and electron diffraction patterns of the electrodeposited iron nanowires, which were separated from AAO nanochannel templates with pore diameters of (a) 85 nm, (b) 67 nm, (c) 52 nm, and (d) 33 nm. The diameters of iron nanowires correspond well to the pore diameters observed in Fig. 1. Considering a membrane thickness of ca. 60 μm, each aspect ratio was determined to be ca. 706, 896, 1154, and 1818, respectively.

Fig. 6 shows X-ray diffraction patterns of iron nanowire arrays that were electrodeposited onto AAO nanochannel templates with average diameters of (a) 85 nm, (b) 67 nm, (c) 52 nm, and (d) 33 nm. The sample with a diameter of 85 nm exhibits a random orientation from (1 1 0) and (2 0 0). All the other samples, by contrast, exhibit a preferred (1 1 0) orientation of bcc-Fe along their longitudinal axis. It is well known that the easiest magnetization direction is [2 0 0] in bcc-Fe crystal. However, in the work, the iron nanowires with pore diameters less than 67 nm exhibited the preferred (1 1 0) orientation. Baik et al. reported that iron nanowires with a single crystalline structure and a preferred (1 1 0) orientation, can be obtained from templates with pore diameters of ca. 63 nm [28]. Hu et al. have also investigated the crystalline reorientation behaviors of bcc iron nanowires which were directly deposited from an acidic chloride electrolyte [29]. They found the iron nanowires with diameters of 30 and 60 nm exhibited the strongest textures with either (1 1 0) or (2 0 0), by controlling the solution pH value. According to the report, bcc-Fe (1 1 0) preferential orientation can be observed in the samples, which were electrodeposited from the aqueous solution of pH2.6 rather than pH3.7. In the present work, the solution pH was kept to 2.0 during the electrodeposition process. Hence, bcc-Fe (1 1 0) preferential orientation was observed in the nanowires with the diameter less than 67 nm in the same manner as the experimental results, which were reported by Hu et al. [29]. It is well known that the lattice spacing of bcc-Fe (1 1 0) is ca. 0.2023 nm at room temperature. Here, in the present work, the characteristic X-ray wavelength of Cu-Kα_1 is 0.154 nm. Thus, bcc-Fe (1 1 0) diffraction peak will be observed at ca. 44.76°. According to Fig. 6, each (1 1 0) diffraction peak, which is obtained from the nanowires with average diameters of 85 nm, 67 nm, 52 nm, and 33 nm, is observed at 44.36°, 43.94°, 44.00° and 44.34°, respectively. Hence, the each (1 1 0) spacing can be determined to 0.2040 nm, 0.2059 nm, 0.2056 nm and 0.2041 nm, respectively. The lattice spacing of bcc-Fe (1 1 0) is larger than that of (2 0 0). Therefore, the lattice spacing extension of (1 1 0) would be more sensitive rather than that of (2 0 0) in the case of interstitial impurities such as hydrogen atoms, which will be induced during the electrodeposition of iron nanowires from an aqueous solution.

Effect of pore diameter on the magnetic performance of iron nanowires

Fig. 7 shows magnetic hysteresis loops of iron nanowire arrays that were electrodeposited onto AAO nanochannel templates with average diameters of (a) 85 nm, (b) 67 nm, (c) 52 nm, and (d) 33 nm, respectively. When the external magnetic field was applied in the axial direction of the nanowires, the coercivity, H_c, and squareness, M_r/M_s (the ratio of remanence and saturation magnetization), increased gradually

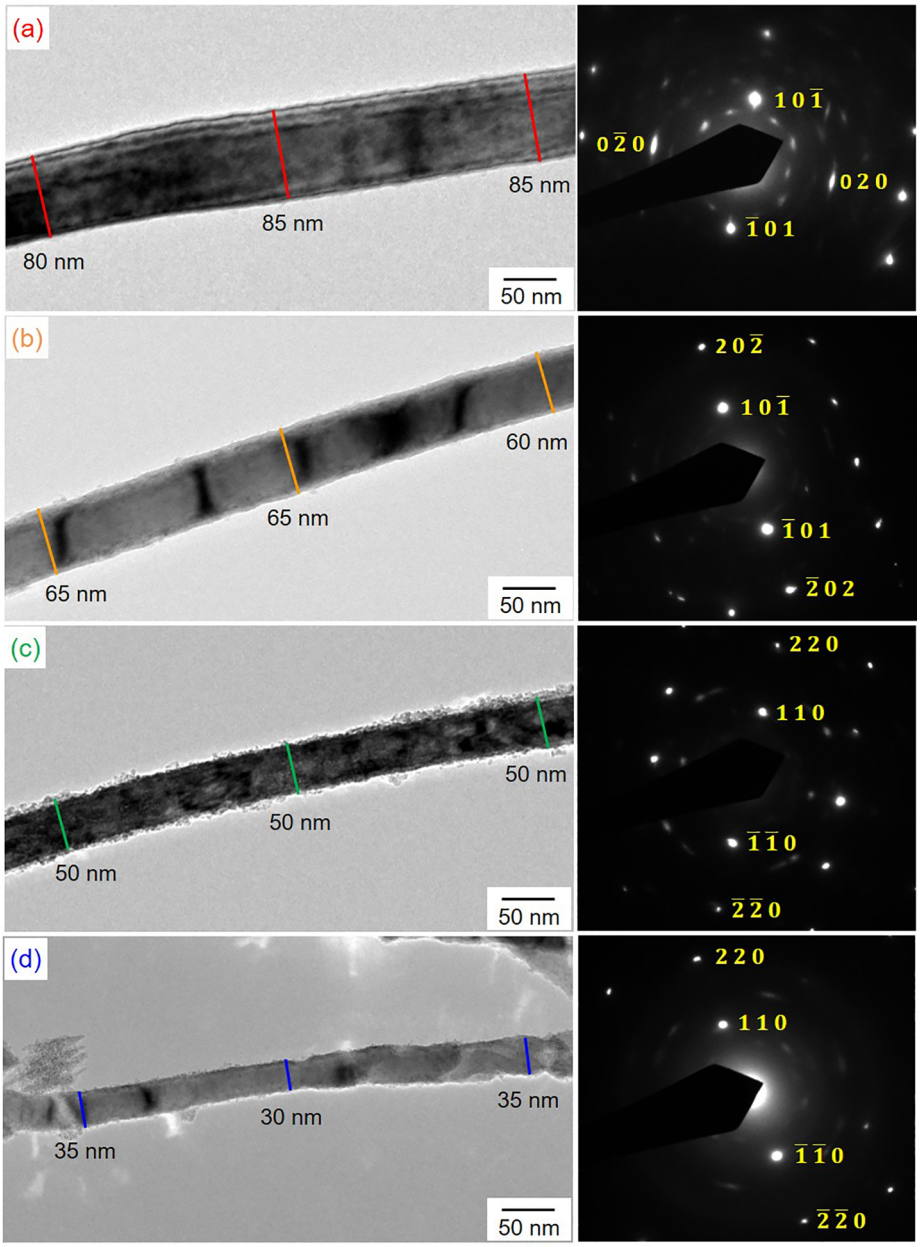

Fig. 5. TEM bright-field images and electron diffraction patterns of electrodeposited iron nanowires, which were separated from AAO nanochannel templates with the pore diameter of 85 nm (a), 67 nm (b), 52 nm (c) and 33 nm (d).

up ca. 1.63 kOe and 0.87, respectively, as the nanowire diameter decreased. On the other hand, when the external magnetic field was applied in the radial direction, the samples were hardly magnetized at all and the squareness was less than 0.3. The effective magnetic anisotropy of iron nanowire arrays can be determined by the magneto-crystalline anisotropy as well as the shape anisotropy of individual nanowires, together with the magneto-static interactions between nanowires. Considering the X-ray diffraction patterns described in Fig. 6, the easiest magnetization direction is along the axial direction of the individual iron nanowires. Thus, the magneto-crystalline anisotropy will be almost constant for the nanowire arrays with diameters less than 67 nm. The shape anisotropies, by contrast, will increase with decreasing pore diameters. Hence, the increase in H_c will be mainly due to the shape anisotropy of iron nanowire arrays.

Fig. 8(a) shows the effect of the diameter on the coercivity of electrodeposited iron nanowire arrays with the magnetic field in the axial and radial direction. Theoretically, a decrease in the demagnetization factor, caused by increasing the aspect ratio (length to diameter), results in an increase in the coercivity [30,31]. In the present work, the coercivity, H_c, increases with decreasing the nanowire diameters, according to the theoretical line plotted by Eq. (2). In the case of iron nanowires, parameters in Eq. (2) are as follows: $A = 2 \times 10^{-6}$ erg/cm

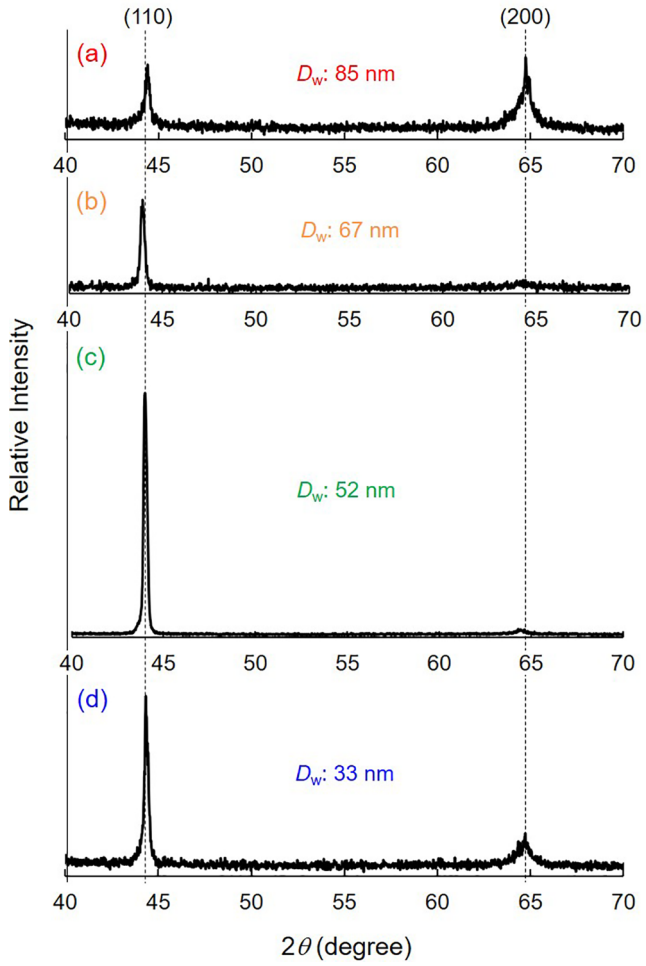

Fig. 6. X-ray diffraction patterns of iron nanowire arrays that were electrodeposited into anodized aluminum oxide nanochannel templates with average diameter of 85 nm (a), 67 nm (b), 52 nm (c) and 33 nm (d).

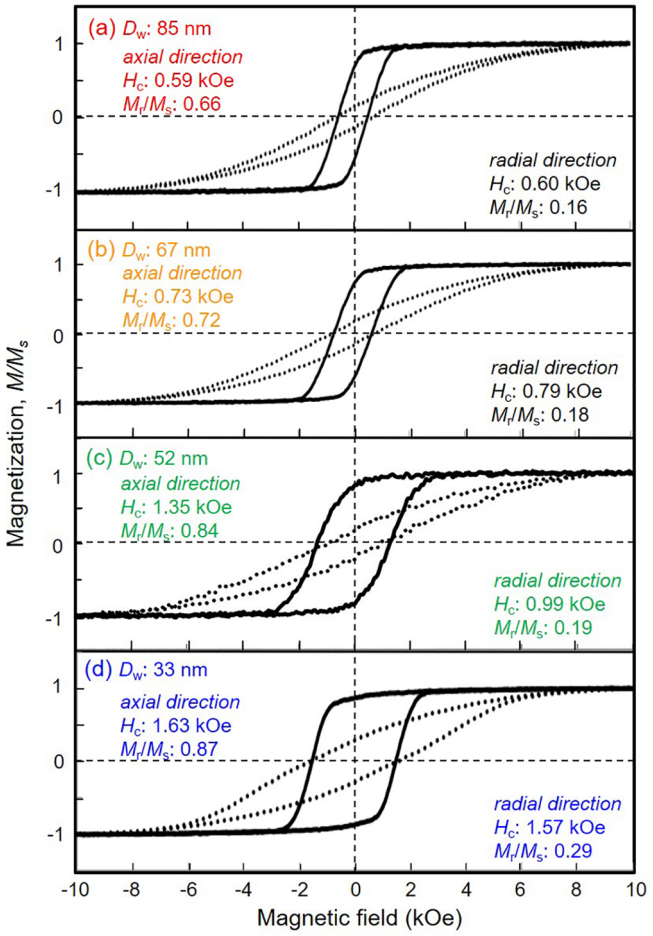

Fig. 7. Magnetic hysteresis loops of iron nanowire arrays that were electrodeposited into anodized aluminum oxide nanochannel templates with average diameter of 85 nm (a), 67 nm (b), 52 nm (c) and 33 nm (d). External magnetic field was applied in the axial direction (solid line) and radial direction (dashed line).

and M_s = 1720 G, where R (in cm) is the radius of the iron nanowires. Hence, the magnetization reversal process in the iron nanowire arrays with aspect ratios of over 1000 seems to be dominated by the magnetization curling mode, which is based on the Shtrikman's micromagnetic theory.

Fig. 8(b) shows the effect of the diameter on the squareness ratios of electrodeposited iron nanowire arrays with the magnetic field in the axial and radial direction. The squareness, M_r/M_s, in the axial direction is quite larger than that in the radial direction because of a decrease in the demagnetization factor, caused by increasing the aspect ratio. Furthermore, it is also found that M_r/M_s increases with decreasing the nanowire diameters due to the extremely large aspect ratio of the individual nanowires.

Conclusion

AAO membranes, which were anodized at 30, 50, 70, and 90 V, showed through-hole architectures with parallel-oriented nanochannels. Each average pore diameter, D_p, was 33, 52, 67, and 85 nm, respectively, for each increasing voltage. Concerning the average interpore distances, D_i, the factor of proportionality f was determined to have been ca. 2.2 nm/V. At the cathode potential of −1.2 V, growth rate of the iron nanowire arrays was determined to be ca. 105 nm s^{-1}, and the maximum aspect ratio reached up to ca. 1800. The iron nanowire arrays with pore diameters less than 67 nm exhibited a preferred (1 1 0) orientation, while those with pore diameters of 85 nm exhibited a random orientation which composed from (1 1 0) and (2 0 0). In the axial direction, iron nanowire arrays were easily magnetized and the squareness, M_r/M_s, reached up to 0.87 with decreasing nanowire diameters. The magnetization reversal process in the iron nanowire arrays was dominated by the magnetization curling mode (Shtrikman's micromagnetic theory) and the coercivity, H_c, increased up to ca. 1.63 kOe with decreasing nanowire diameters.

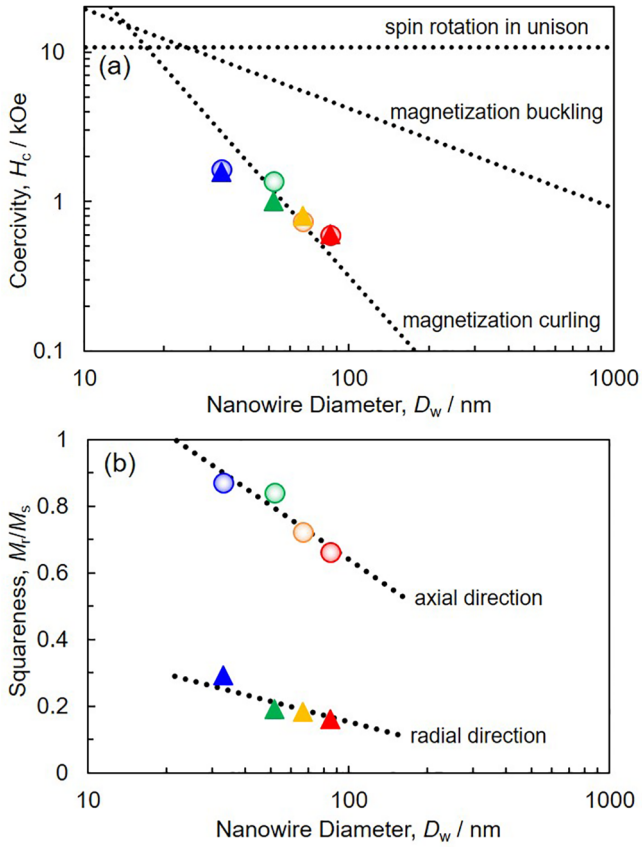

Fig. 8. Effect of the diameter on the coercivity (a) and squareness ratio (b) of electrodeposited iron nanowire arrays with the magnetic field in the axial (○) and radial (△) direction.

Acknowledgements

The authors thank Japan Science and Technology Agency, Japan (JST: AS262Z02450K), the Japan Society for the Promotion of Science, Japan (JSPS: PE14005, 15K06508 and 18H01754) and IKETANI Science and Technology Foundation, Japan (0271040-A) for the financial support.

References

[1] Duguet E, Vasseur S, Mornet S, Devoisselle J-M. Magnetic nanoparticles and their applications in medicine. Nanomedicine 2006;1(2):157–68.
[2] Matsui I. Nanoparticles for electronic device applications. J Chem Eng Jpn 2005;38(8):535–46.
[3] Ai Z, Deng K, Wan Q, Zhang L, Lee S. Facile microwave-assisted synthesis and magnetic gas sensing properties of Fe_2O_4 nanoroses. J Phys Chem C 2010;114(14):6237–42.
[4] Mou F, Guan J, Ma H, Xu L, Shi W. Magnetic iron oxide chestnutlike hierarchical nanostructures: preparation and their excellent arsenic removal capabilities. ACS Appl Mater Interfaces 2012;4(8):3987–93.
[5] Kharisov BI, Dias HVR, Kharissova OV, Jiménez-Pérez VM, Pérez BO, Flores BM. Iron-containing nanomaterials: synthesis, properties, and environmental applications. ACS Adv 2012;2:9325–58.
[6] Wu H, Zhang R, Liu X, Lin D, Pan W. Electrospinning of Fe Co, and Ni nanofibers: synthesis, assembly, and magnetic properties. Chem Mater 2007;19(14):3506–11.
[7] Ji G, Tang S, Xu B, Gu B, Du Y. Synthesis of $CoFe_2O_3$ nanowire arrays by sol-gl-template method. Chem Phys Lett 2003;379(5–6):484–9.
[8] Hu MJ, Lin B, Yu SH. Magentic field-induced solvothermal synthesis of one-dimensional assemblies of Ni-Co alloy microstructuures. Nano Res 2008;1(18):303–13.
[9] Borissov D, Isik-Uppenkamp S, Rohwerder M. Fabrication of iron nanowire arrays by electrodeposition into porous alumina. J Phys Chem C 2009;113(8):3133–8.
[10] Ohgai T, Washio R, Tanaka Y. Anisotropic magnetization behavior of electrodeposited nanocrystalline Ni-Mo alloy thin films and nanowires array. J Electrochem Soc 2012;159(10):H800–4.
[11] Apel P. Track etching technique in membrane technology. Radiat Meas 2001;34(1–6):559–66.
[12] Jani AMM, Losic D, Voelcker NH. Nanoporous anodic aluminum oxide: advances in surface engineering and emerging applications. Prog Mater Sci 2013;58:636–704.
[13] Ohgai T, Hoffer X, Gravier L, Ansermet J-Ph. Electrochemical surface modification of aluminium sheets for application to nano-electronic devices: anodization aluminium and electrodeposition of cobalt-copper. J Appl Electrochem 2004;34(10):1007–12.
[14] Haehnel V, Faehler S, Schaaf P, Miglierini M, Mickel C, Schultz L, et al. Towards smooth and pure iron nanowires grown by electrodeposition in self-organized alumina membranes. Acta Mater 2010;58:2330–7.
[15] Rosa WO, Vivas LG, Pirota KR, Asenjo A, Vázquez M. Influence of aspect ratio and anisotropy distribution in ordered CoNi nanowire arrays. J Magn Magn Mater 2012;324(24):3679–82.
[16] Neetzel C, Ohgai T, Yanai T, Nakano M, Fukunaga H. Uniaxial magnetization performance of Co-Al_2O_3 nano-composite films electrochemically synthesized from acidic aqueous solution. J Solid State Electrochem 2016;20(6):1665–72.
[17] Wang W, Li N, Li X, Geng W, Qiu S. Synthesis of metallic nanotube arrays in porous anodic aluminum oxide template through electroless deposition. Mater Res Bull 2006;41(8):1417–23.
[18] Jia Y, Wang H, Gao Y, Chen P, Lu J, Han G. Magnetostatic interaction in FeCo nanowire arrays. J Magn Magn Mater 2014;374:417–22.
[19] Liu QF, Gao CX, Xiao JJ, Xue DS. Size effects on magnetic properties in $Fe_{0.68}Ni_{0.32}$ alloy nanowire arrays. J Magn Magn Mater 2003;260:151–5.
[20] Zeng H, Skomski R, Menon L, Liu Y, Bandyopadhyay S, Sellmyer DJ. Structure and magnetic properties of ferromagnetic nanowires in self-assembled arrays. Phys Rev B 2002;65:13446.
[21] Frei EH, Shtrikman S, Treves D. Critical size and nucleation field of ideal ferromagnetic particles. Phys Rev 1957;106(3):446–55.
[22] Neetzel C, Ohgai T, Yanai T, Nakano M, Fukunaga H. Uniaxial magnetization performance of textured Fe nanowire arrays electrodeposited by a pulsed potential deposition technique. Nanoscale Res Lett 2017;12:598.
[23] Juan JH, He FY, Sun DC, Xia XH. A simple method for preparation of through-hole porous anodic alumina membrane. Chem Mater 2004;16:1841–4.
[24] Belwalkar A, Grasing E, Van Geertruyden W, Huang Z, Misiolek WZ. Effect of processing parameters on pore structure and thickness of anodic aluminum oxide (AAO) tubular membranes. J Membr Sci 2008;319:192–8.
[25] Bai A, Hu C-C, Yang Y-F, Lin C-C. Pore diameter control of anodic aluminum oxide with ordered array of nanopores. Electrochim Acta 2008;53:2258–64.
[26] Poinern GEJ, Ali N, Fawcett D. Progress in nano-engineered anodic aluminum oxide membrane development. Materials 2011;4:487–526.
[27] Sulka GD, Brzózka A, Zaraska L, Jaskuła M. Through-hole membranes of nanopores alumina formed by anodizing in oxalic acid and their applications in fabrication of nanowire arrays. Electrochim Acta 2010;55:4368–76.
[28] Baik JM, Schierhorn M, Moskovits M. Fe nanowires in nanoporous alumina: geometric effect versus influence of pore walls. J Phys Chem C 2008;112:2252–5.
[29] Hu HN, Chen HY, Chen JL, Wu GH. Magnetic properties of (110)- and (200)-oriented Fe-nanowire arrays. Phys B 2005;368:100–4.
[30] Schloerb H, Haehnel V, Khatri MS, Srivastav A, Kumar A, Schultz L, et al. Magnetic nanowires by electrodeposition within templates. Phys Status Solidi B 2010;247(10):2364–79.
[31] Metzger RM, Konovalov VV, Sun M, Xu T, Zangari G, Xu B, et al. Magnetic nanowires in hexagonally ordered pores of alumina. IEEE Trans Magn 2000;36(1):30–5.